Control of multiphoton and avalanche ionization using an ultraviolet-infrared pulse train in femtosecond laser micro-/nano-machining of fused silica

Xiaoming Yu[a], Qiumei Bian[a], Zenghu Chang[b], P.B. Corkum[c,d], Shuting Lei[a]
[a]Industrial and Manufacturing Systems Engineering, Kansas State University, Manhattan, Kansas 66506, USA
[b]College of Optics & Photonics and Department of Physics, University of Central Florida, Orlando, Florida 32816, USA
[c]National Research Council of Canada, Ottawa, Ontario K1A 0R6, Canada
[d]University of Ottawa, Ottawa, Ontario K1N 6N5, Canada

ABSTRACT

We report on the experimental results of micro- and nanostructures fabricated on the surface of fused silica by a train of two femtosecond laser pulses, a tightly focused 266 nm (ultraviolet, UV) pulse followed by a loosely focused 800 nm (infrared, IR) pulse. By controlling the fluence of each pulse below the damage threshold, micro- and nanostructures are fabricated using the combined beams. The resulting damage size is defined by the UV pulse, and a reduction of UV damage threshold is observed when the two pulses are within ~ 1 ps delay. The effects of IR pulse duration on the UV damage threshold and shapes are investigated. These results suggest that the UV pulse generates seed electrons through multiphoton absorption and the IR pulse utilizes these electrons to cause damage by avalanche process. A single rate equation model based on electron density can be used to explain these results. It is further demonstrated that structures with dimensions of 124 nm can be fabricated on the surface of fused silica using 0.5 NA objective. This provides a possible route to XUV (or even shorter wavelength) laser nano-machining with reduced damage threshold.

1. INTRODUCTION

The interaction between femtosecond laser pulses and dielectric materials involves complicated processes, such as free electron excitation and decay, exciton generation, plasma absorption, energy transfer from electrons to lattices, hydrodynamics, shockwave propagation, damage formation, etc [1-12]. Understanding these processes is of great importance for potential application of femtosecond lasers in optical storage, micro-/nano-fluidics, opto-electronics and nanomachining [13-17].

Free electron generation, among these processes, is believed to play a crucial role in the interaction between femtosecond laser pulses and dielectric materials [3-6]. On one hand, it is the first process occurring in a femtosecond laser pulse duration because electrons have a high charge-mass ratio compared to ions and thus are easier to move correspondingly with the electric field of a laser pulse. The initial free electrons are generated by photo-ionization (multi-photon and/or tunneling, depending on the laser intensity and band structure). These initially built-up free electrons can further absorb energy from laser pulses through inverse bremsstrahlung and produce more free electrons from the valence band by collision ionization. This process continues for the pulse duration, and therefore an electron avalanche occurs. Electrons generated from both photo and avalanche ionization form a plasma gas, and it is found that the majority of energy is absorbed by this plasma during laser-material interaction [18]. On the other hand, the density of these free electrons, n_e, is a key parameter in determining the damage threshold for a laser pulse. According to the Drude model, the plasma angular frequency, ω_p, relates to n_e as follows,

$$\omega_p = \sqrt{\frac{n_e e^2}{\varepsilon_0 m_e}}, \tag{1}$$

where e is electron charge, ε_0 is vacuum permittivity, and m_e is electron mass. ω_p increases with n_e, and when it approaches the laser angular frequency, ω_l, the absorption abruptly increases and it is believed that damage occurs at this point [19]. The corresponding electron density is the critical density (1.7×10^{21} cm^{-3} for fused silica and 800 nm pulses).

Laser-based Micro- and Nanoprocessing VIII, edited by Udo Klotzbach, Kunihiko Washio, Craig B. Arnold,
Proc. of SPIE Vol. 8968, 89680G · © 2014 SPIE · CCC code: 0277-786X/14/$18 · doi: 10.1117/12.2035290

This free electron dynamics, to some extent, determines the following processes, such as energy transfer from electrons to lattices and eventually the formation of damage. This motivates us to investigate this electron dynamics and apply it for machining purposes.

Pump-probe experiments are a commonly used technique in the fundamental studies of laser-material interaction, in which a higher energy (pump) pulse interacts with materials and a lower energy pulse is used to probe the process. One can get various information by observing the change of probe pulse's energy, phase, etc, and effectively series of snapshots of the process can be taken with sub-picosecond to femtosecond resolution [20]. In pump-probe experiments, the energy of probe pulses is kept as low as possible to avoid interference with pump pulses. Recent studies employing double (multiple) pulse techniques in femtosecond laser micromachining, on the contrary, use a high energy probe pulse to control the dynamics of free electrons generated by a pump pulse. Results from these experiments show that the second pulse enhances ablation rates and lowers damage threshold of the first pulse. These results suggest that free electrons generated by the first pulse are able to absorb energy from the second pulse.

Although the enhancement effects by double- (multi-) pulse experiments have been studied, applying this technique to fabricate features with sub-micron size is not yet reported. Feature size is fundamentally controlled by diffraction limit, λ/NA, where λ is laser wavelength and NA is the numerical aperture of focusing optics. Although structures with size of 130 nm and 200 nm are achieved by high NA microscope objectives [21, 22], smaller features are not easy to get because NA for non oil-immersion objectives is smaller then one. And also high NA optics generally have short working distance, which is not preferred in machining applications, because debris can easily attach to optic surfaces, affect laser beam delivery and even damage optics. Alternatively, using short wavelength lasers, such as UV range, feature sizes of 250 nm on fused silica and 600 nm on stainless steel foils have been reported [23, 24]. Even shorter wavelength, such as XUV and X-ray can be obtained by HHG. Although the conversion efficiency of HHG is low, fortunately, the required pulse energy for generating sub-micron size features is on the order of nano Joule, and such energy has already been achieved by recent experiments [25]. Shorter wavelength laser pulses have higher photon energy, and thus are more easily to promote electrons from valence band to conduction band by photo-ionization. Therefore, it is possible to use a short wavelength pulse to produce seed electrons and a long wavelength pulse to cause electron avalanche. With help of the long wavelength pulse, the damage threshold of the short wavelength pulse may be reduced. Because short wavelength pulses, such as XUV and X-ray, are difficult to get and the conversion efficiency is low, reducing the damage threshold means that the same beam can be divided into several beams and thus machining speed will be multiplied. And since the volume of excited free electrons is controlled by the short wavelength pulse, the resulting damage size will be similar to that generated by the short wavelength alone. With the advance of XUV and X-ray optics, direct machining with resolution of tens of nanometer or even smaller can be achieved.

In this paper, we present the experimental and modeling results of micro-/nano-machining using a UV-IR pulse train. In Section 2, we investigate the relationship between UV damage threshold and UV-IR pulse delay, and demonstrate that the damage size is controlled by the UV pulse. A rate equation model is used to explain the experimental results. In Section 3, the effects of IR pulse duration is studied, and an optimal IR pulse duration is found. In Section 4, damage as small as 124 nm is achieved by focusing the UV pulse with a 0.5 NA reflecting objective lens.

2. DOUBLE-PULSE MICROMACHINING

In the first step to demonstrate the concept of double-pulse machining, we combine 266 nm (UV) and 800 nm (IR) pulses [26]. The experimental setup is shown in Figure 1. The UV pulses are produced by third harmonic generation (THG). Both UV and IR beams are focused onto a fused silica sample (Corning 7980) by two lenses with 50 mm and 200 mm focal length, respectively. The resulting focal spot size is 9.2 μm and 25.4 μm. A delay stage is used to change the delay between these two beams. A BBO crystal is placed near the focal points to verify the delay. Zero delay is set when the strongest difference frequency generation (DFG) is observed.

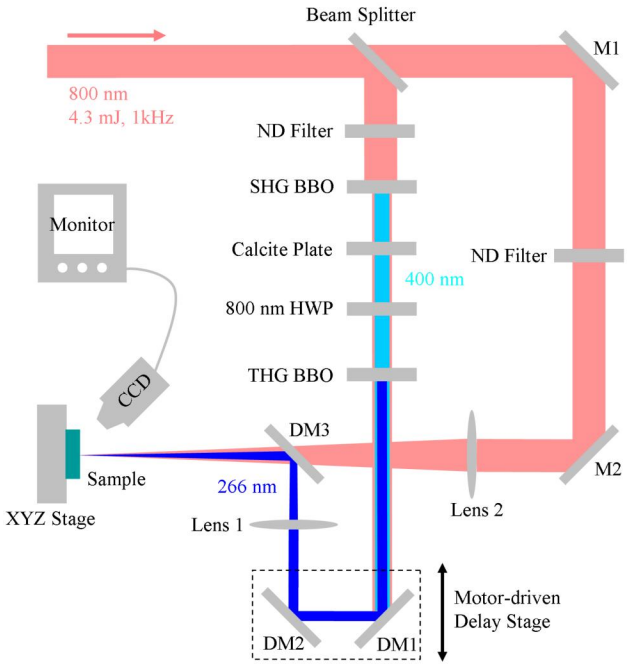

Figure 1. Experimental setup for UV-IR double pulse machining. [26]

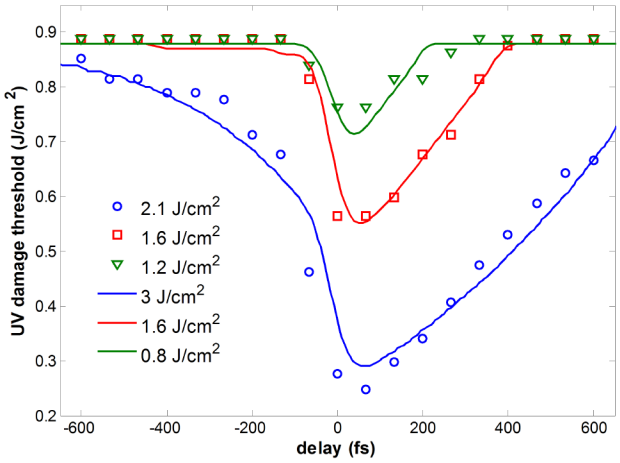

Figure 2. Dependence of UV damage threshold on the time delay at different IR fluences. Dots: experimental data. Curves: simulation data. α_{UV} = 2 cm^2/J, α_{IR} = 0.9 cm^2/J, $t_{p,UV}$ = 70 fs, $t_{p,IR}$ = 60 fs, τ = 250 fs, $n_{critical}$ = 1.7×10^{21}/cm^3. [26]

Figure 2 shows the relationship between UV damage threshold and UV-IR pulse delay at three IR fluences. Positive delays mean UV pulses reach the sample before IR pulses. It can be seen that at the highest IR fluence, UV damage threshold reaches 0.25 J/cm^2 at 60 fs delay, 28% of the normal value. A lower IR fluence increases UV damage threshold, but an "optimal delay" exists for all three cases. This can be explained using a simple rate equation model given below:

$$\frac{dn}{dt} = W_{PI}(I_{UV}) + \alpha_{UV} I_{UV} n + W_{PI}(I_{IR}) + \alpha_{IR} I_{IR} n - \frac{n}{\tau}, \tag{2}$$

where n is free electron density, W_{PI} is the multiphoton ionization rate calculated from the Keldysh theory, α_{UV} and α_{IR} are the avalanche ionization rates for UV and IR pulses, respectively, τ is the electron recombination time, and I_{UV} and I_{IR} are the intensity for UV and IR pulses, respectively. Our modeling results show similar relationship as the experimental results.

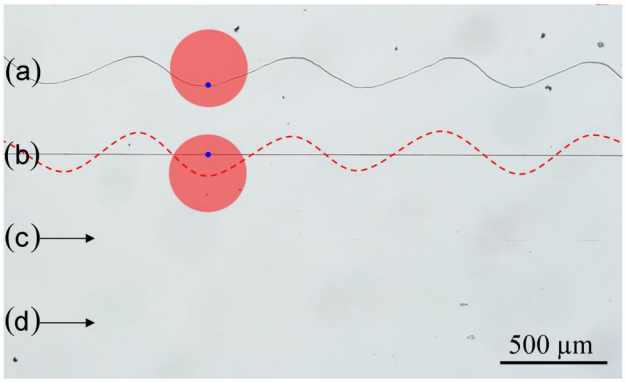

Figure 3. Optical images of different structures fabricated by a combination of UV and IR pulses. (a) Moving UV spot while keeping IR spot fixed. (b) Moving IR spot while keeping UV spot fixed. No structure can be seen using either (c) UV or (d) IR beam individually to write straight lines.

To demonstrate that the damage size is defined by the seeding UV beam, we write different lines as shown in Figure 3. The IR focal spot is deliberately enlarged to 330 µm, much larger than the UV spot (9.2 µm). In Figure 3(a), the UV spot is moving vertically while the IR spot is fixed. In Figure 3(b), on the contrary, IR spot is moving and the UV spot is fixed. It can be seen that in both cases, damage lines follow the movement of the UV beam, which indicates that indeed the damage is controlled by the seeding UV beam.

3. EFFECTS OF IR PULSE DURATION

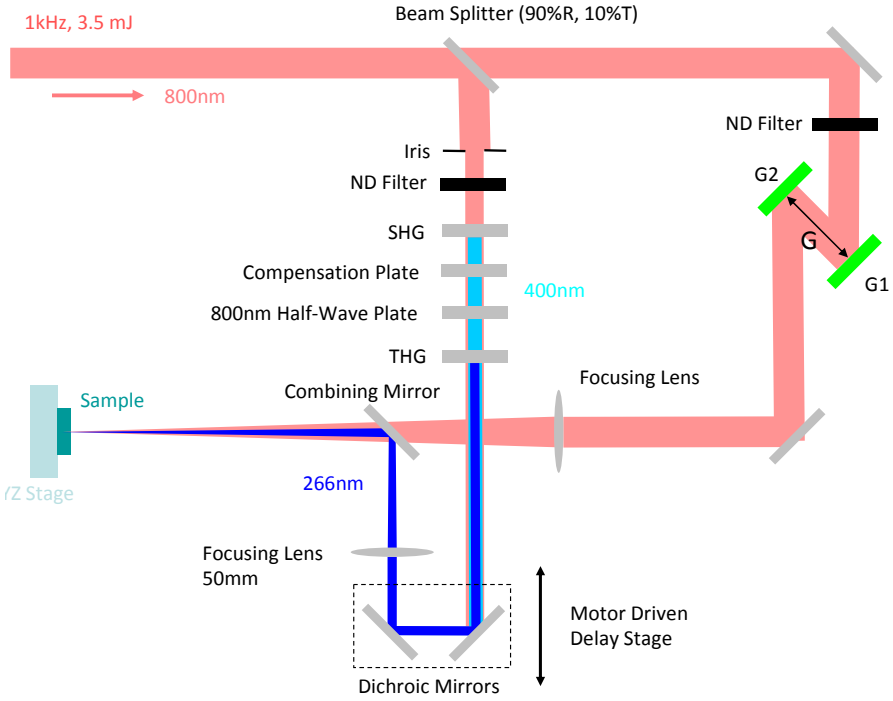

Figure 4. Experimental setup for study of the effects of IR pulse duration.

Once excited, free electrons can further absorb energy from laser field by inverse bremsstrahlung, and this results in electron avalanche (avalanche ionization, AI). Our previous results show that with the combination of UV and 60 fs IR pulses, UV damage threshold can be lowered by 70%. Since free electrons are continuously produced as long as laser irradiation exists, a long IR pulse duration may help generate more free electrons and therefore further reduce UV damage threshold. Motivated by this idea, we combine 70 fs UV pulses with IR pulses that have different pulse duration (60 fs ~ 1.87 ps), as shown in Figure 4. A single-pass grating pair consisting of G1 and G2 (900 lines/mm, d=1.11 μm) is used to stretch the IR pulse with transform limited pulse duration (τ) of 60 fs. The stretched pulse duration (τ_s) is calculated by

$$\tau_s = \tau\sqrt{1+\left(\frac{4\ln 2\cdot\varphi_2}{\tau^2}\right)^2}, \tag{3}$$

where φ_2 is second order group delay dispersion, which is calculated by

$$\varphi_2 = -\frac{G}{d^2}\frac{\lambda^3}{2\pi c^2}\frac{1}{\cos^2\theta_d}, \tag{4}$$

where G is the distance between gratings, d is grating constant (1.11 μm), λ is wavelength (800 nm), c is the speed of light, and θ_d is diffraction angle (1.2º for first order). Due to the space limitation, the shortest duration of stretched pulses by this grating pair is 490 fs. For shorter pulse duration, three cube polarizers with a total thickness of 65 mm are used, and the calculated pulse duration is 120 fs. It should be noted that the grating pair produces negative chirp, while the polarizers result in positive chirp, and spatial chirp in the grating pair is not compensated. UV and IR pulses are combined at zero delay by observing the difference frequency generation (DFG) by the UV and IR pulses. Single shot UV damage threshold is defined as the lowest UV pulse energy which causes visible damage under an optical microscope. Five IR pulse durations are used, 60 fs, 120 fs, 490 fs, 1 ps and 1.87 ps. The IR pulse energy for each pulse duration is kept at 5% below the normal damage threshold.

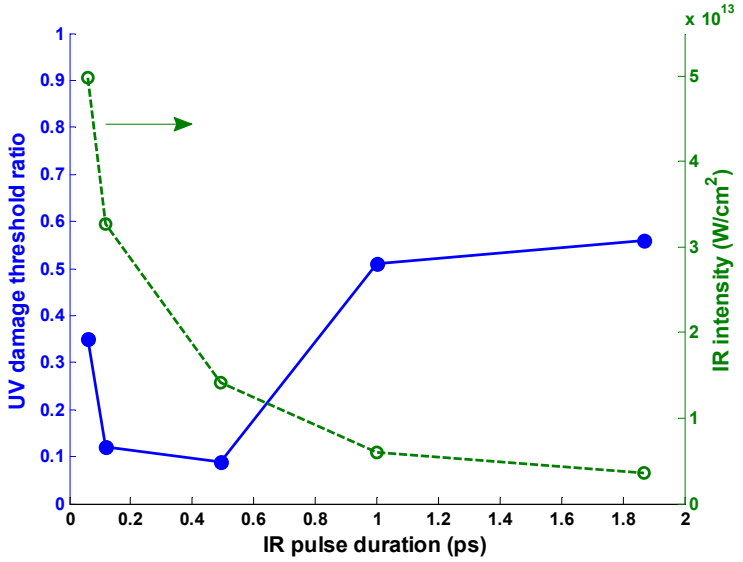

Figure 5. UV damage threshold ratio and IR pulse intensity at different IR pulse durations.

For different IR pulse durations, the single shot UV damage threshold ratio, which is defined as the ratio of the damage threshold with and without combining the IR pulse, is shown in Figure 5. It is found that the lowest damage threshold is obtained with 490 fs IR pulse duration, which is only 9% of the normal threshold value. This can be explained as follows. On one hand, a long pulse duration enhances energy absorption of free electrons by extending the duration of absorption and thus helps decrease UV damage threshold. On the other hand, it is found that for the single IR beam, the damage

threshold fluence for the 1.87 ps pulse duration is only 2.2 times that for 60 fs, although the pulse duration is more than 30 times longer. This means that in order to avoid damage caused by the IR beam, the intensity for 1.87 ps is only 7% of that for 60 fs. The actual IR intensity used in the experiments is also shown in Figure 5. Since the avalanche ionization is intensity dependent (αIn), a lower intensity reduces the ionization rate and thus increases UV damage threshold. The overall shape of the UV damage threshold curve is perhaps due to the balance of these two mechanisms.

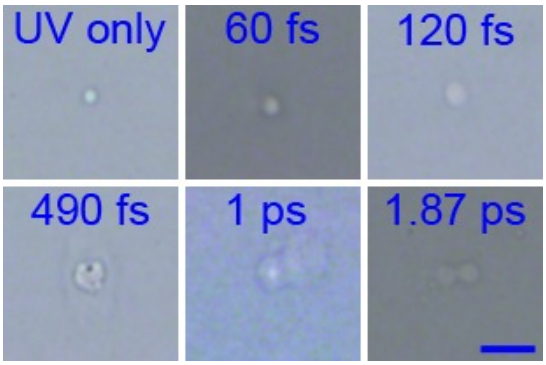

Figure 6. Comparison of the smallest damage size for different IR pulse durations. Scale bar is 10 μm.

In the UV-IR double pulse experiments, the damage shape is controlled by the seeding UV pulse, as shown in Figure 3. However, with longer IR pulse durations, we observe a trend of increasing size of the smallest damage, as shown in Figure 6. The five IR pulse durations are the same as in Figure 5, and the UV spot size is the same in all cases. A damage by the UV pulse only is also shown for comparison. It can be seen that a single UV beam produces the smallest size, and with the UV-IR pulse train, a longer IR pulse duration produces generally a larger size (60 – 490 fs). With pulse duration of 1 ps and 1.87 ps, damage shapes are different from those of shorter pulse durations. Please note that in the case of 490 fs, the IR fluence is slightly higher than its damage threshold, so the IR pulse already cause damage. These results are preliminary and need further verification from both experimental and theoretical aspects.

4. NANOMETER DAMAGE ACHIEVED BY SINGLE UV BEAM

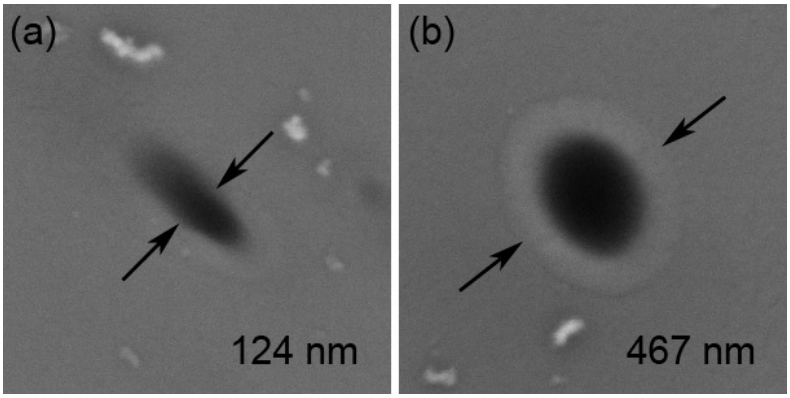

Figure 7. SEM images of damage caused by a single UV pulse. In (a) and (b), the sample is placed at two different positions along the beam propagation direction. The damage size is measured along the direction indicated by the arrows.

With wavelength one third of the fundamental 800 nm beam, the 266 nm beam generated from THG can be used to produce nanometer damage when focused by moderate NA optics. Here we use a reflecting objective lens (Edmund) with NA of 0.5 and working distance of 23.3 mm to focus the UV beam. The results are shown in Figure 7. Probably due to the bad profile of the 266 nm beam and lack of optimization of the reflecting objective in UV range, the damage shape varies along the beam propagation direction. Nonetheless, damage size as small as 124 nm is obtained [Figure 7(a), measured along the narrowest direction]. This suggests that by improving the UV profile and optimizing the objective, damage can be easily controlled in 100 nm scale. Our recent results show that the double-pulse setup (described in Section 2) can also be applied in nanomachining, and the UV damage threshold can be lowered by an order [27].

5. CONCLUSION

In this paper, we demonstrate the possibility of controlling multiphoton and avalanche ionization by a UV-IR pulse train. UV damage threshold can be reduced by an order with the help of IR pulses, and the damage size is controlled by the seeding UV pulse. Longer IR pulse duration can enhance the energy absorption, while a trend of increasing damage size is observed. Damage size with 124 nm (on one direction) is obtained by focusing the 266 nm beam with an 0.5 NA reflecting objective. With shorter wavelength beams, e.g., XUV and X-ray, resolution below 10 nm can be achieved, and the required energy is below the normal damage threshold when combined with a longer wavelength beam.

This material is based on work supported by the Army Research Office and the National Science Foundation under Grant Number 1068604.

REFERENCES

[1] R. R. Gattass, and E. Mazur, "Femtosecond laser micromachining in transparent materials," Nature Photon. **2**, 219 (2008).
[2] D. Grojo, M. Gertsvolf, S. Lei, T. Barillot, D. M. Rayner, and P. B. Corkum, "Exciton-seeded multiphoton ionization in bulk SiO(2)," Phys. Rev. B **81**, 212301 (2010).
[3] M. Li, S. Menon, J. P. Nibarger, and G. N. Gibson, "Ultrafast Electron Dynamics in Femtosecond Optical Breakdown of Dielectrics," Phys. Rev. Lett. **82**, 2394 (1999).
[4] M. Lenzner, Kr, uuml, J. ger, S. Sartania, Z. Cheng, C. Spielmann, G. Mourou, W. Kautek, and F. Krausz, "Femtosecond Optical Breakdown in Dielectrics," Phys. Rev. Lett. **80**, 4076 (1998).
[5] L. Sudrie, A. Couairon, M. Franco, B. Lamouroux, B. Prade, S. Tzortzakis, and A. Mysyrowicz, "Femtosecond Laser-Induced Damage and Filamentary Propagation in Fused Silica," Phys. Rev. Lett. **89**, 186601 (2002).
[6] B. C. Stuart, M. D. Feit, A. M. Rubenchik, B.W. Shore, and M. D. Perry "Laser-induced demages in dielectrics with nanosecond to picosecond pulses " Phys. Rev. Lett. **74**, 2248 (1995).
[7] A. Mermillod-Blondin, J. Bonse, A. Rosenfeld, I. V. Hertel, Y. P. Meshcheryakov, N. M. Bulgakova, E. Audouard, and R. Stoian, "Dynamics of femtosecond laser induced voidlike structures in fused silica," Appl. Phys. Lett. **94**, 041911 (2009).
[8] Y. Hayasaki, M. Isaka, A. Takita, and S. Juodkazis, "Time-resolved interferometry of femtosecond-laser-induced processes under tight focusing and close-to-optical breakdown inside borosilicate glass," Opt. Express **19**, 5725-5734 (2011).
[9] T. Y. Choi, D. J. Hwang, and C. P. Grigoropoulos, "Femtosecond laser induced ablation of crystalline silicon upon double beam irradiation," Appl. Surf. Sci. **197**, 720-725 (2002).
[10] L. Jiang, and H.-L. Tsai, "A plasma model combined with an improved two-temperature equation for ultrafast laser ablation of dielectrics," J. Appl. Phys. **104**, 093101 (2008).
[11] P. Balling, and J. Schou, "Femtosecond-laser ablation dynamics of dielectrics: basics and applications for thin films," Rep. Prog. Phys. **76**, 036502 (2013).
[12] E. G. Gamaly, and A. V. Rode, "Physics of ultra-short laser interaction with matter: From phonon excitation to ultimate transformations," Prog. Quant. Electron. **37**, 215-323 (2013).
[13] L. Canioni, M. Bellec, A. Royon, B. Bousquet, and T. Cardinal, "Three-dimensional optical data storage using third-harmonic generation in silver zinc phosphate glass," Opt. Lett. **33**, 360-362 (2008).
[14] Y. Liao, Y. Shen, L. Qiao, D. Chen, Y. Cheng, K. Sugioka, and K. Midorikawa, "Femtosecond laser nanostructuring in porous glass with sub-50 nm feature sizes," Opt. Lett. **38**, 187-189 (2013).
[15] J.-H. Klein-Wiele, and P. Simon, "Sub-wavelength pattern generation by laser direct writing via repeated irradiation," Opt. Express **21**, 626-630 (2013).
[16] Y. V. White, X. Li, Z. Sikorski, L. M. Davis, and W. Hofmeister, "Single-pulse ultrafast-laser machining of high aspect nano-holes at the surface of SiO2," Opt. Express **16**, 14411 (2008).
[17] M. K. Bhuyan, F. Courvoisier, P. A. Lacourt, M. Jacquot, R. Salut, L. Furfaro, and J. M. Dudley, "High aspect ratio nanochannel machining using single shot femtosecond Bessel beams," Appl. Phys. Lett. **97**, 081102-081103 (2010).
[18] N. Varkentina, N. Sanner, M. Lebugle, M. Sentis, and O. Utéza, "Absorption of a single 500 fs laser pulse at the surface of fused silica: Energy balance and ablation efficiency," J. Appl. Phys. **114**, - (2013).
[19] L. Jiang, and H. Tsai, "Energy transport and material removal in wide bandgap materials by a femtosecond laser pulse," Int. J. Heat Mass Transfer **48**, 487 (2005).

[20] D. J. Hwang, C. P. Grigoropoulos, and T. Y. Choi, "Efficiency of silicon micromachining by femtosecond laser pulses in ambient air," J. Appl. Phys. **99**, 083101-083106 (2006).
[21] S. I. Kudryashov, G. Mourou, A. Joglekar, J. F. Herbstman, and A. J. Hunt, "Nanochannels fabricated by high-intensity femtosecond laser pulses on dielectric surfaces," Appl. Phys. Lett. **91**, 141111 (2007).
[22] J. M. Fernández-Pradas, C. Florian, F. Caballero-Lucas, J. L. Morenza, and P. Serra, "Femtosecond laser ablation of polymethyl-methacrylate with high focusing control," Appl. Surf. Sci. **278**, 185 (2013).
[23] D. N. Nikogosyan, M. Dubov, H. Schmitz, V. Mezentsev, I. Bennion, P. Bolger, and A. V. Zayats, "Point-by-point inscription of 250-nm-period structure in bulk fused silica by tightly-focused femtosecond UV pulses: experiment and numerical modeling," Cent. Europ. J. Phys. **8**, 169-177 (2009).
[24] J. Békési, J. H. Klein-Wiele, and P. Simon, "Efficient submicron processing of metals with femtosecond UV pulses," Appl. Phys. A **76**, 355-357 (2003).
[25] Y. Wu, E. Cunningham, H. Zang, J. Li, M. Chini, X. Wang, Y. Wang, K. Zhao, and Z. Chang, "Generation of high-flux attosecond extreme ultraviolet continuum with a 10 TW laser," Appl. Phys. Lett. **102**, 201104-201104 (2013).
[26] X. Yu, Q. Bian, B. Zhao, Z. Chang, P. B. Corkum, and S. Lei, "Near-infrared femtosecond laser machining initiated by ultraviolet multiphoton ionization," Appl. Phys. Lett. **102**, 101111-101114 (2013).
[27] X. Yu, Q. Bian, Z. Chang, P. B. Corkum, and S. Lei, "Femtosecond laser nanomachining initiated by ultraviolet multiphoton ionization," Opt. Express **21**, 24185-24190 (2013).